

Figure 7: Map of the star-forming regions selected in the six central fields; the radii of the circles are proportional to the size of the regions. Ages (in 10^6 yr) of the youngest stars found in the C-M diagrams are indicated.

is accurate enough to get an estimate of the ages of the single regions. We have used models calculated for a solar metallicity and adopted the internal absorption values given by SC. A larger extinction correction had to be adopted for star-forming regions belonging to the central parts of the galaxy. An example of the procedure is shown in Figure 6.

We find that the youngest stars of

NGC 3109 have ages of the order of $\sim 6 \times 10^6$ years, with masses $\sim 30 M_\odot$; in other words, this galaxy is still active in forming stars. Moreover, since the part of the diagrams corresponding to ages of 20–100 million years appears rather uniformly populated by stars, we may conclude that, in this time interval, stars have formed in an almost regular manner (see the plot in Fig. 7, where

sizes and ages of the selected regions are shown). A comparison with similar work on other resolved DIGs shows that the level of recent star formation in NGC 3109 is quite high, a fact which is probably related to the size of the galaxy.

Acknowledgements

We are indebted to thank G. Bertelli, C. Chiosi, and E. Nasi, for providing us with the isochrones for the massive stars in advance of publication. We also thank S. Ortolani for the Danish observations.

References

- Capaccioli, M., Ortolani, S., and Piotto, G., 1987, in Proceedings of the ESO Workshop on "Stellar Evolution and Dynamics in the Outer Halo of the Galaxy", eds. M. Azzopardi and F. Matteucci, p. 281.
- Demers, S., Kunkel, W.E., and Irwin, M.J., 1985, *Astron. J.* **90**, 1967.
- de Vaucouleurs, G., and Freeman, K.C., 1972, *Vistas Astron.* **14**, 163.
- Humphreys, R.M., 1983, *Astrophys. J.* **269**, 335.
- Hunter, D.A., and Gallagher, J.S., 1985, *Astrophys. J. Suppl. Ser.* **58**, 533.
- Landolt, A.U., 1983a, *Astron. J.* **88**, 439.
- Landolt, A.U., 1983b, *Astron. J.* **88**, 853.
- Piotto, G., King, I.R., Capaccioli, M., Ortolani, S., and Djorgovski, S., 1990, *Astrophys. J.* **350**, 662.
- Sandage, A., and Carlson, G., 1988, *Astron. J.* **96**, 1599.
- Stetson, P.B., 1987, *P.A.S.P.* **99**, 191.
- Trimble, V., 1987, *Ann. Rev. Astron. Astrophys.* **25**, 67.

Probing the Hidden Secrets of Seyfert Nuclei

I. APPENZELLER and S. WAGNER, Landessternwarte Heidelberg-Königstuhl, F.R. Germany

The nuclei of active galaxies are clearly among the most spectacular and violent places that can be found in our present universe. Most extreme are the bright Quasars, where we observe a total energy output equivalent to a large galaxy cluster from galactic core regions comparable in size to our solar system. In addition to optical and radio radiation we often observe intense X-ray and even energetic Gamma radiation as well as collimated streams of matter moving at velocities close to the velocity of light.

Most current theories assume that the enormous radiation power of active galactic nuclei (AGNs) is produced by massive rotating black holes residing in the dynamical centres of these galaxies. Swallowing surrounding material at

rates up to about one earth mass per second, such black holes give rise to huge rotating magnetic fields and electric current systems which can explain the astonishing properties of these systems.

However, in spite of a large research effort during the past decades we are still lacking a reliable observational confirmation of the basic physical models of the AGNs and our knowledge of the detailed physical processes occurring in AGNs is still highly incomplete. One reason for the slow progress of our understanding of the AGNs is the great distance of most active galaxies which makes it impossible to resolve the active nuclei by direct imaging techniques. Furthermore, during the past decade it

became increasingly evident that in many AGNs the central engines are not directly visible but hidden behind opaque dusty matter concentrations along the line of sight. Even in the case of nearby Seyfert galaxies (the nearest known examples of AGNs), direct optical radiation from the centre of the active nuclei seems to be observed only in exceptional cases. Moreover, when direct radiation is detected, it is often mixed with light of the normal stellar galactic core and with emission from circum-nuclear normal HII regions ionized by stars.

Fortunately, modern observing techniques provide various methods to overcome some of the observational difficulties mentioned above. High-resolution

spectroscopy often allows to separate the different components which contribute to the (on direct images) unresolved galactic cores. When the galactic cores are hidden from us by local dust absorption, their radiation fields can sometimes be determined indirectly from its effects on the interstellar gas in the host galaxies. Finally, recent progress in infrared imaging techniques makes it possible to penetrate part of the absorbing dust layers and to look deeper into the hidden central regions of the AGNs.

In this paper we shall report about our experience with these methods at the ESO telescopes during various recent observing runs. Because of limited space we shall restrict this report mainly to results on the two particularly interesting emission line galaxies NGC 5728 and IC 5063. NGC 5728 is a prominent barred spiral with a Seyfert 2 nucleus. An account of its basic properties and a photographic image of this galaxy can be found in an earlier issue of the *Messenger* (cf. [1]). IC 5063 (= PKS 2048-572) is an early-type radio galaxy known mainly for its pronounced dust lanes. In addition to data on these two galaxies, a few results on the prototype Seyfert 2 galaxy NGC 1068 will be reported.

Improving the Angular Resolution by Means of Spectroscopy

In the optical spectral range AGNs are usually identified by the characteristic emission line spectra produced in their Broad-Line and Narrow-Line Regions (BLRs and NLRs). Compared to most stellar spectra even the NLR spectral features are rather broad and have Doppler widths of several hundred km s^{-1} or more. Hence, on first glance it seems not to make sense to observe these spectra with high spectral resolution. However, as illustrated by Figure 1, high resolution spectra of AGNs can in fact provide important information. The upper part of Figure 1 shows long-slit spectrograms of the $\text{H}\alpha$ and $[\text{NII}]$ 6584 Å lines of NGC 5728 obtained with the ESO CASPEC spectrograph. The horizontal coordinate corresponds to wavelength (expressed as a relative Doppler velocity) while the vertical coordinate gives the location of the emission along the projected spectrograph slit. The centres of the two long slit spectra correspond (in velocity) to the systemic velocity of NGC 5728 (as derived from the absorption lines of the stellar component) and (in space) to the dynamical centre of the galaxy. Hence, a monochromatic light source emitting the corresponding spectral lines and moving with the centre of NGC 5728 would pro-

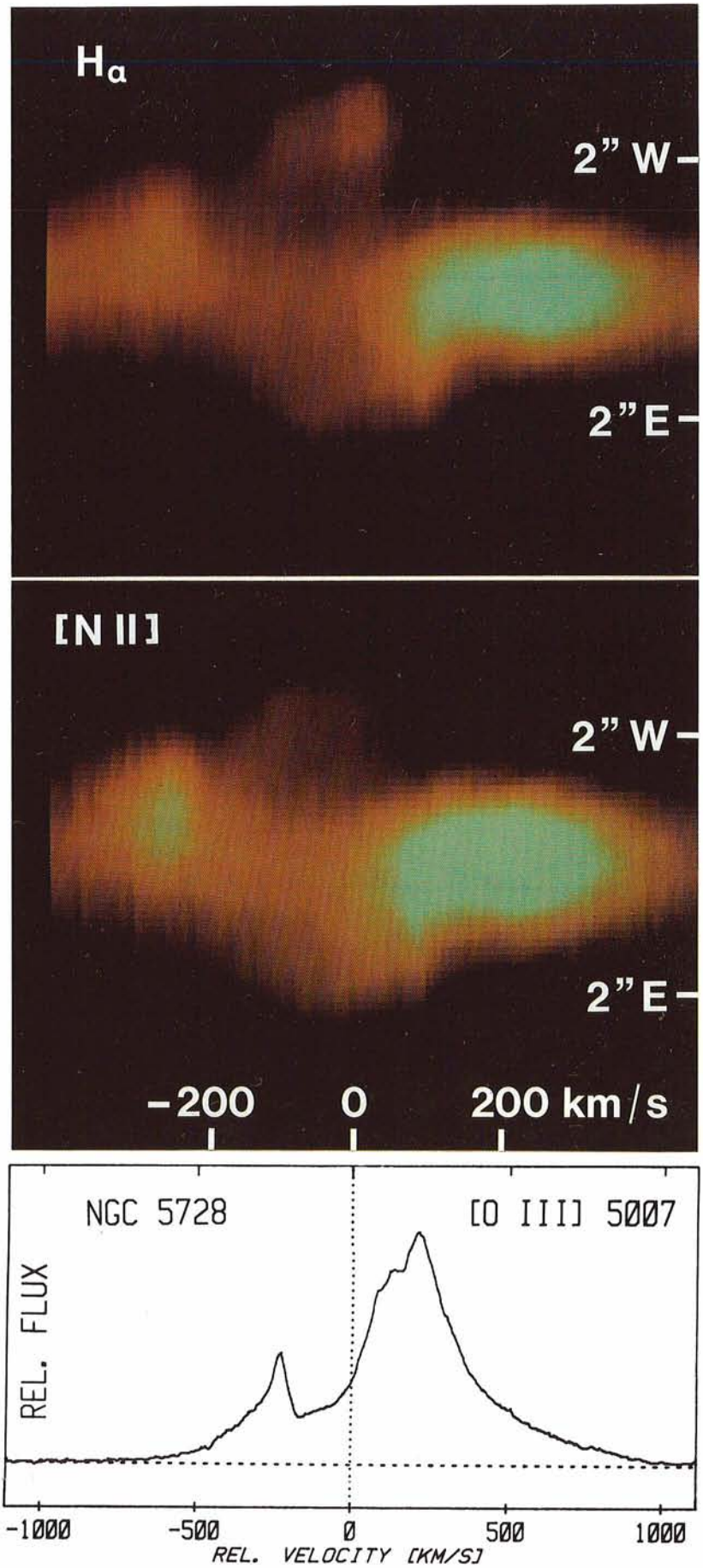


Figure 1: Emission-line profiles of the nucleus of NGC 5728. On top are long-slit spectrograms of the cores of the $\text{H}\alpha$ and $[\text{NII}]$ 6584 profiles, obtained with an EW slit orientation. Below is a tracing (obtained by integrating along the slit) of the full $[\text{OIII}]$ 5007 profile.

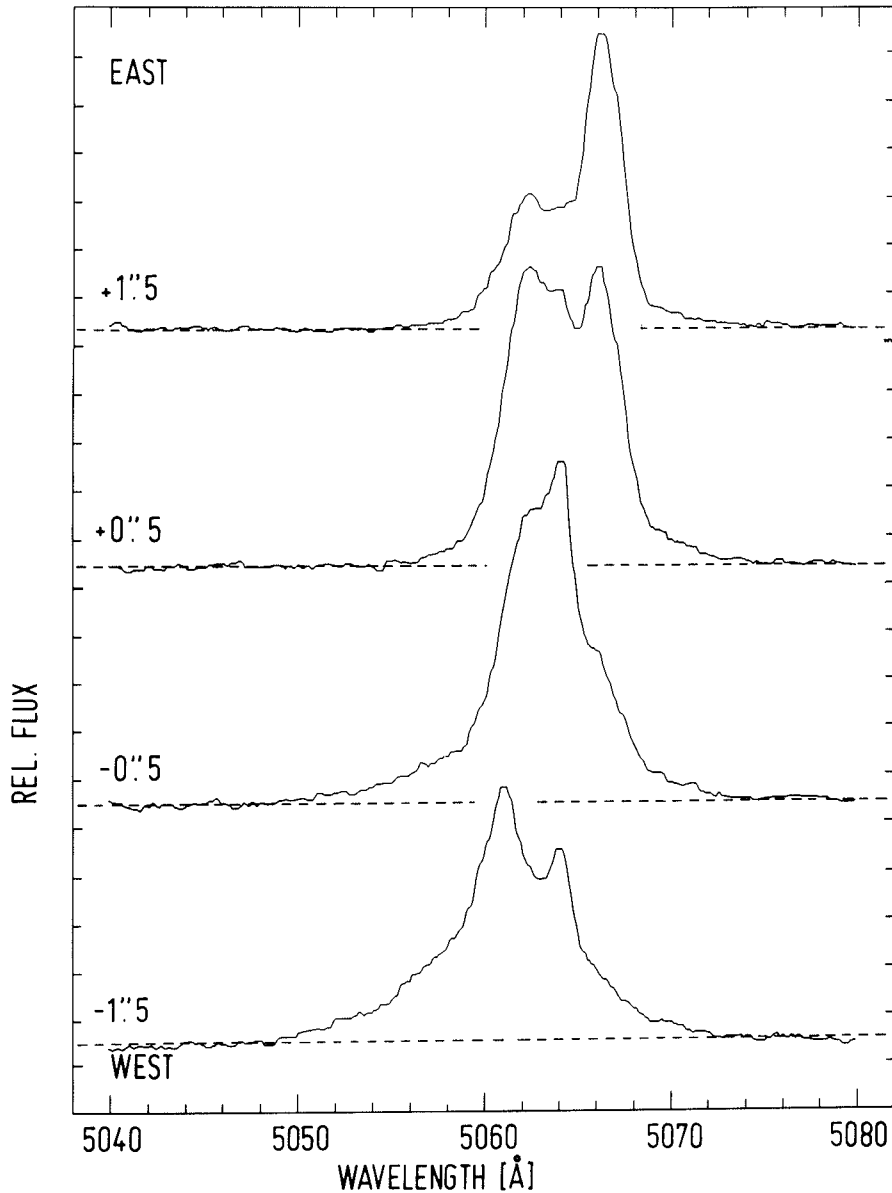


Figure 2: Emission-line profiles at different angular displacements from the core of IC 5063.

duce a point in the centre of each of the two images, while an extended monochromatic source would produce a vertical line.

As shown in Figure 1, due to the violent motion of the nuclear gas the line emission is distributed over a significant velocity range, producing the characteristic complex line profiles of the NLR (cf. [2]). Moreover, the emission is also smeared out in spatial direction. Although atmospheric seeing contributes to this spatial extension, Figure 1 (obtained with $\leq 0''.8$ seeing) clearly shows that much of the observed spatial extent is caused by the superposition of individual emission regions with different velocities and spatial locations. The highly different relative intensities of the individual components in the two line profile images show that the emitting gas volumes vary greatly in their phys-

ical conditions. As most of these emission components are concentrated in the innermost two arcseconds of the nucleus they cannot be resolved on direct images but become visible only on long slit spectrograms of sufficient spectral resolution.

A more detailed investigation (cf. [3]) shows that most of the emission line regions seen in Figure 1 correspond to measurably extended volumes of gas. Only the strongest component shows the angular intensity distribution of an unresolved point source. This component must correspond to the true Seyfert nucleus. Surprisingly, the nuclear emission, although projected on the dynamical centre of the galaxy, does not have the systemic velocity of the galaxy but shows a velocity shift of more than 200 km s^{-1} . This velocity shift is even more conspicuous in the tracing of the

[O III] 5007 Å line (lower part of Figure 1), where the unresolved component corresponds to the redshifted peak.

A velocity difference of more than 200 km s^{-1} between the whole NLR and the dynamical centre of its host galaxy appears highly unlikely in all current AGN models. Hence, it seems much more plausible to explain the spectroscopic results by assuming that in the case of NGC 5728 only the red wing of the NLR profiles is observed, while the matter producing the rest of the NLR profile (i.e., in fact, most of the NLR) is hidden from us by dust absorption. With a slightly larger amount of dust absorption NGC 5728 could probably not even be recognized as an active galaxy.

Another example of the effects of circumnuclear dust in an AGN is shown in Figure 2, where we reproduce line profile tracings obtained for points on the major axis of the galaxy IC 5063 at various distances from the centre of the active nucleus. As the line again contains contributions of different volumes with different line widths and radial velocities, the NLR profile changes with distance from the centre. A surprising detail of Figure 2 is the fact that the profile observed at the centre is relatively narrow, while conspicuous broad line wings are present about $1''.5$ (corresponding to about 500 pc at the distance of IC 5063) NW of the dynamical centre. By separating the observed profiles into individual emission components, it can be shown that the broad wings are produced by a local emission region with a velocity width of about 900 km s^{-1} (cf. [4]). Such broad line components are expected to form only in the central regions of AGNs. The fact that such a broad emission profile is found from a region far outside the centre strongly suggests that we observe nuclear light which is scattered by dust clouds which are located outside the nuclear region and which are exposed to radiation from the nucleus. Since no broad wings are detected in the radiation reaching us from the direction of the nucleus, we again have to conclude that along our line of sight the core of the AGN is hidden by dust and that only indirect radiation is able to reach us at visible wavelengths.

The ENLR Connection

In addition to producing scattered light, the intense radiation field of the AGNs can also ionize the interstellar matter of their host galaxies. Depending on the UV flux and the matter distribution, the ionization effect may be significant even at distances of many kpc from the nucleus. The resulting “extended narrow line regions” (ENLRs) show the

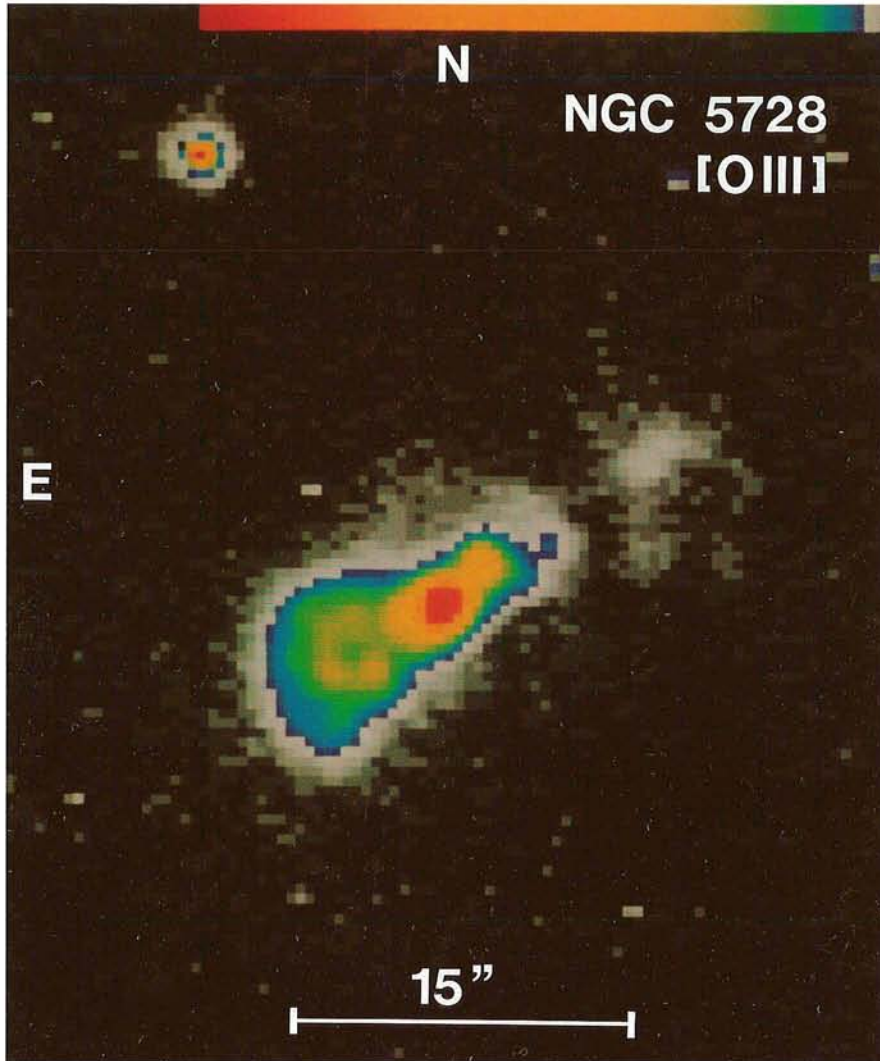


Figure 3: False-colour map of the extended [OIII] emission of NGC 5728.

same (nonthermal) ionization characteristics as the nuclear NLRs (and thus are easily distinguished from normal HII regions), but (due to lower internal velocities) differ from the NLRs by much narrower line profiles.

Figure 3 shows the ENLR of NGC 5728 as outlined by its [OIII] emission. As demonstrated by the figure, most of the observed ENLR emission is found in two relatively narrow cones extending towards the SE and NW directions from the nucleus. Interestingly, the axis defined by these two cones also coincides (at least in projection) with a jet-like region of enhanced radio emission (cf. [5]). Such coaxial morphologies have also been found for other AGNs and have been interpreted as evidence for central radiation fields and relativistic particle flows directed mainly parallel to the rotation axis of the nucleus, while the radiation perpendicular to the rotation axis is blocked by a disk of dusty gas clouds. If this explanation is correct, and if the radiation cones of NGC 5728 are indeed oriented as suggested by Figure 3, it is obviously no surprise that little direct

radiation from the centre of this AGN is visible in our line of sight.

Infrared Imaging

Since the scattering and absorption cross sections of typical interstellar dust grains decrease with increasing wavelengths, dust absorption is most severe in blue images of galaxies and becomes less important at red and infrared wavelengths. Therefore, dust absorption features are usually traced most efficiently by means of "ratio images" which are generated by calculating the ratios of corresponding pixels of two images obtained at different wavelengths. An example, showing the ratio between a visual (V-band) image and near-infrared (I-band) image of IC 5063 (observed by C. Möllenhoff and P. Surma), is given in Figure 4. As the dust absorption is weaker in the I-band (corresponding to about $0.85 \mu\text{m}$) than in the V-image (central wavelength $\approx 0.55 \mu\text{m}$) dust features appear darker in the ratio image. Figure 4 shows a particularly prominent dust lane just north of the nucleus. Since it almost coincides with the nucleus, it certainly affects the light reaching us from the core of this galaxy. The nucleus itself appears in the ratio image as a double peak. This is readily explained by the fact that its visual image is (due to stronger dust absorption) and a stronger contribution of extended line emission in the V-band) elongated while its I image is more circular.

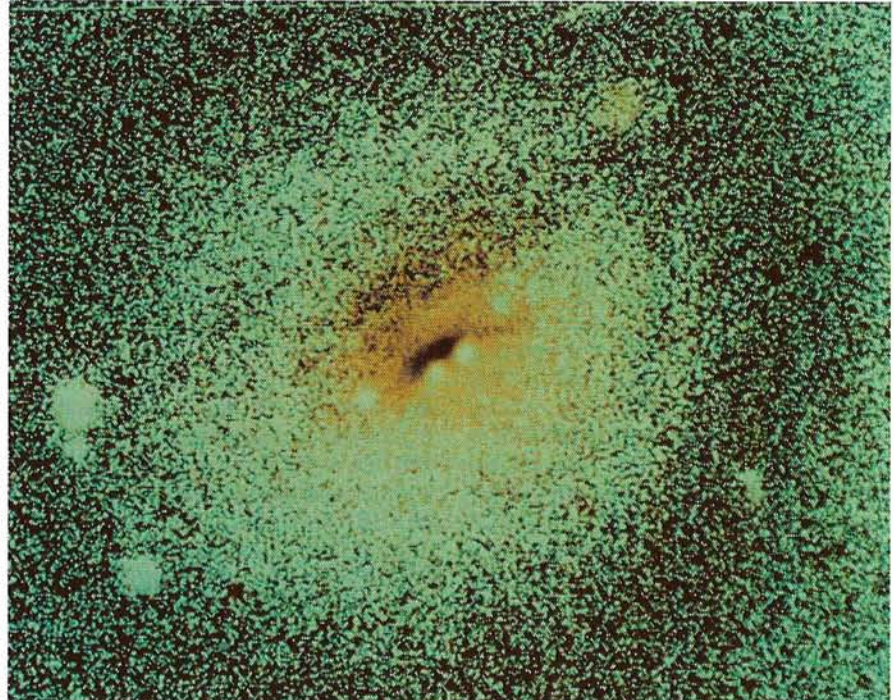


Figure 4: V/I ratio map of the central part of IC 5063. The image covers about $2' \times 2.5'$. North is up, east to the left.

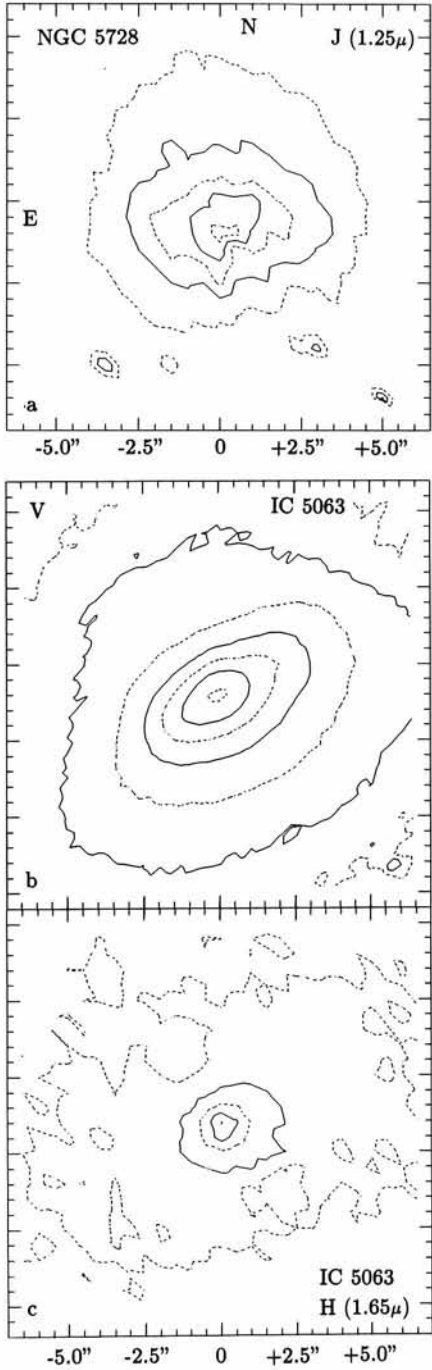


Figure 5: Examples of broad-band images of the cores of NGC 5728 and IC 5063.

The ratio image of Figure 4 shows that I-band images (corresponding to the longest wavelength band that can be efficiently observed with normal Si CCD detectors) are clearly less affected by dust absorption than blue and visual images. However, a detailed analysis of our I-image shows that the dust lanes can still be traced even at these wavelengths and that the morphology seen in the I-band image is still influenced by the dust absorption. In order to look behind the dust, one obviously has to observe at even longer wavelengths. Therefore, we recently

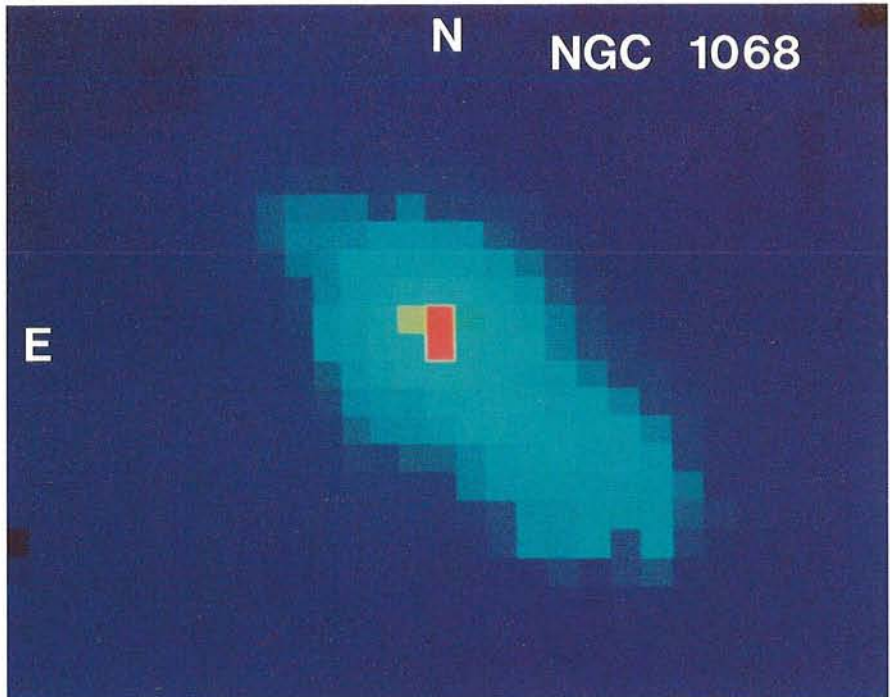


Figure 6: False-colour map of the Brackett-gamma emission from the core of NGC 1068. The continuum has been subtracted by means of an image obtained in an adjacent narrow line-free continuum band. The image covers a field of $38'' \times 48''$.

used ESO's new IRAC infrared array camera (cf. [6], [7]) to obtain images of several dusty Seyfert nuclei in the J ($1.25 \mu\text{m}$), H ($1.65 \mu\text{m}$), and K ($2.2 \mu\text{m}$) bands. Because of poor weather conditions and various technical deficiencies of the 32×32 pixel HgCdTe array available to us, our run was only a partial success. In the case of NGC 5728 only J-band images of sufficient S/N could be obtained. The IC 5063 observations were more successful, yielding images of reasonably good S/N in all three continuum bands and with different field sizes.

Examples of isophote maps derived from our IR images of the core regions of NGC 5728 and IC 5063 are presented in Figure 5a and c. In Figure 5b we show for comparison a V-band isophote map of the same area of IC 5063. Both IR isophote maps are based on images obtained with circular pixels of about $0''.16$ diameter with a $0''.5$ spacing. The (FWHM) resolution (limited by the seeing) is about $1''.2$. The V map (based on $0''.35$ densely packed and quadratic pixels) has a resolution of about $1''.5$.

As illustrated by Figure 4, in the case of NGC 5728 most of the observed radiation in the $1.2 \mu\text{m}$ band is emitted from a slightly elongated extended region with an average diameter of about $7''$ (corresponding to about 2 kpc). This region agrees well (in size, shape and orientation) with the area inside the ring of gas and stars which delineates the core of NGC 5728 on optical images (cf.

[3]). Although the J-band emission reaches its maximum intensity in the centre, no distinct point source corresponding to the nucleus can be detected. The (in Figure 5 omitted) lower-intensity outer contours of the J-band intensity distribution become elongated along the (NE-SW) Major axis of the galaxy, indicating a low-level background produced by the stellar component. The extended IR radiation from the core region is probably also dominated by starlight, although extended line emission (e.g. of the Paschen lines of hydrogen) may contribute.

More interesting are the maps obtained for IC 5063. In all three IR-bands the observed radiation was found to consist of three distinct components. As illustrated by Figure 5c, the outer contours show an elongation along the major axis of the galaxy. The corresponding low-level extended emission again seems to originate from the stellar component. Superimposed is a small, about circular extended (diameter $\approx 4''$) region which surrounds a prominent unresolved central point source. There seems to be little doubt that this IR point source corresponds to the Seyfert nucleus of IC 5063. A comparison of the V and the H maps of Figure 5 shows that the conspicuous isophote distortion by the dust lanes visible in the V map cannot be detected in the IR image, suggesting that absorption by these features is no longer significant at this wavelength. However, this has to be

confirmed by a more detailed analysis of all three infrared frames.

The physical interpretation of the observed extended nuclear IR emission of IC 5063 is again complicated by the presence of emission lines in the three observed infrared bands. A separation of the line and continuum contribution requires narrower pass bands. Such narrow bands can be realized with the circular variable filter (CVF) of the IRAC camera. However, the detector noise of the present array limits this mode of operation to relatively bright objects. From published IR line fluxes only the nearby Seyfert 2 galaxy NGC 1068 appeared to be bright enough to attempt CVF observations. As this galaxy also belongs to the AGNs with evidence for a hidden core (cf. [8]) NGC 1068 was also included in our programme.

Our broad-band IR images of NGC 1068 show qualitatively similar proper-

ties as the IC 5063 frames. We again observe a bright unresolved nucleus surrounded by extended emission. Surprisingly, our narrow-band CVF images in line-free IR continuum bands turned out to be quite different. These images show the unresolved central nucleus but practically no detectable continuum radiation from an extended circumnuclear region. On the other hand, as demonstrated by the Brackett-gamma line image reproduced in Figure 6, in the light of the IR emission lines we clearly see also extended emission surrounding the nucleus. Hence, in the case of NGC 1068 it seems clear that at least most of the extended circumnuclear IR emission is caused by line emitting gas.

Our results for NGC 1068 clearly demonstrate the potential of narrow-band IR imaging for studies of nearby AGNs. Hopefully, improved array detectors and larger telescopes will make it possible to apply this technique in the

future also to other active galaxies including the hidden cores discussed in the first chapters of this paper.

References

- [1] van Gorkom, J.H., Kotanyi, C.G., Tarenghi, M., Véron-Cetty, M.P., Véron, P.: 1983, *The Messenger* **33**, 37.
- [2] Appenzeller, I., Östreicher, R.: 1988, *Astron. J.* **95**, 45.
- [3] Wagner, S.J., Appenzeller, I.: 1988, *Astron. Astrophys.* **197**, 75.
- [4] Wagner, S.J., Appenzeller, I.: 1989, *Astron. Astrophys.* **225**, L13.
- [5] Schommer, R.A., Caldwell, N., Wilson, A.S., Baldwin, J.A., Phillips, M.M., Williams, T.B., Turtle, A.J.: 1988, *Astrophys. J.* **324**, 154.
- [6] Moorwood, A.: 1988, *The Messenger* **52**, 50.
- [7] Moorwood, A., Finger, G., Moneti, A.: 1988, *The Messenger* **54**, 56.
- [8] Antonucci, R.R.J., Miller, J.S.: 1985, *Astrophys. J.* **297**, 621.

A Redshift Survey of Automatically Selected Clusters of Galaxies

L. GUZZO¹, R. NICHOL², C. COLLINS³, S. LUMSDEN⁴

¹Osservatorio di Brera, Milan, Italy; ²Department of Astronomy, University of Edinburgh, Great Britain;

³Royal Observatory, Edinburgh, Great Britain; ⁴Astrophysics Group, Imperial College, London, Great Britain

Introduction

The study of the large-scale structure of the universe provides direct constraints on the initial form of the density fluctuations from which galaxies, clusters and superclusters formed. This can be achieved by mapping the large-scale galaxy distribution, with the assumption that light is a good tracer of the underlying mass distribution. To compare our maps with the theory, we need to extract some numbers describing their properties in a statistical sense. One of the main properties which are of interest in this sense is *clustering*, i.e. how the distribution of objects differs from a random sample. This is of great importance, since theories usually give precise predictions about the level of clustering on different scales.

The most popular statistical estimator of clustering is certainly the two-point spatial correlation function $\xi(r)$, that measures the probability in excess of random of finding two objects at a separation r (see Peebles, 1980). One of the most remarkable results obtained in the last few years is that the two-point correlation function for clusters of galaxies

(ξ_{cc}) is about 15 times stronger than that for galaxies (ξ_{gg}) (see Bahcall, 1988). This observation is one piece of evidence that has prompted the idea of biased galaxy formation (Kaiser, 1984) and indicates that neither galaxies nor clusters can both be tracers of the mass distribution. In the context of models of galaxy formation the "standard cold dark matter" model (CDM) fails to provide enough power on cluster scales when normalized to fit the observed ξ_{gg} (White et al., 1987).

Given the prime importance of this observation, it is extraordinary that we still rely on estimates of the cluster correlation function based on "eyeball" catalogues of clusters, namely the Abell (1957) and Abell, Corwin, Olowin (ACO, 1989) lists. Evidence has been accumulating about systematic and unquantifiable selection effects present in such visual compilations, giving rise to doubts on the reality of the observed ξ_{cc} (Sutherland, 1988, and see Dekel, 1989 for discussion). With these uncertainties in mind, the estimation of ξ_{cc} from a redshift survey of objectively (i.e. automatically) detected clusters is long over-

due. In 1988 we started at ESO a redshift survey based on an automatic sample of rich clusters extracted from the Edinburgh/Durham Southern Galaxy Catalogue. The results (so far) have been very successful, and in this note we would like to report on the present status of the project.

The Automatic Catalogue of Clusters

As mentioned, the cluster catalogue has been extracted from the Edinburgh/Durham Southern Galaxy Catalogue (EDSGC), one of the first ever large-scale machine-based optical galaxy catalogues. This galaxy survey has been constructed using the COSMOS high-speed microdensitometer, and consists of 60 UK Schmidt J survey plates centred at the South Galactic Pole. The galaxy catalogue covers an area of 0.5 steradians to a limiting magnitude of $b_J = 20$, with a total of ~ 1.5 million galaxies, with $> 95\%$ completeness and $< 10\%$ star contamination (see Heydon-Dumbleton, Collins and MacGillivray, 1989 for details). The EDSGC represents an ideal